Proceedings 10th NUMGE 2023
10th European Conference on Numerical Methods in Geotechnical Engineering
Zdravkovic L, Kontoe S, Taborda DMG, Tsiampousi A (eds)

https://doi.org/10.53243/NUMGE2023-179

Micro-mechanical response of transversely isotropic samples under cyclic loading

M. Salimi[1], M. Tafili[1], N. Irani[1], T. Wichtmann [1]

[1]*Chair of Soil Mechanics, Foundation Engineering and Environmental Geotechnics, Ruhr University of Bochum, Bochum, Germany*

ABSTRACT: This study aims to identify the effect of inherent anisotropy (bedding plane inclination) and mechanisms affecting the susceptibility of granular soils to liquefaction by utilizing the three-dimensional discrete element method (DEM). A set of simulations were carried out on transversely isotropic particulate assemblies as well as isotropic sample under undrained cyclic constant total mean pressure conditions varying the inherent anisotropy and deviatoric stress loading amplitude. Simulations highlight the combined impact of shear stress amplitude and anisotropic microstructure of the assemblies on the liquefaction potential, post-liquefaction displacement, coordination number, and accumulation of excess pore-water pressure. In addition, the results show that the preferential particle elongation and contact anisotropy of particles at liquefaction are highly dependent on the predefined anisotropy direction. It turns out, that the inherent anisotropy affects the undrained cyclic resistance.

Keywords: constant total stress; inherent anisotropy; cyclic; undrained; DEM

1 INTRODUCTION

Investigation of the soil response under repeated loading is indispensable in geotechnical engineering as many civil structures are subjected to multiple unloading-reloading cycles such as machine foundations (Calvetti et al., 2010), bridge footings (Elgamal et al., 2008), tunnels (Tafili and Wichtmann, 2022) piles (Machaček et al., 2021) and the foundations of wind turbines (Krathe and Kaynia, 2017). While many research has focused on the drained and undrained soil response under recurring loading of isotropic samples (e.g., Wichtmann and Triantafyllidis, 2014, 2016; Li et al., 2020; Knittel et al., 2022), limited knowledge is available concerning the cyclic response of soils with inherent anisotropy. The profound role of anisotropy has been indicated in decreasing the bearing capacity of shallow foundations located on transversely isotropic granular soil (Azami et al. 2010; Qin et al. 2016), strain localization in soil specimens (Lu et al., 2011) and may cause a significant deviation from the strength design (Li and Dafalias, 2002).The amplitude of deviatoric stress and strain (Chiaro et al., 2012), initial stress state (Araei et al., 2012), void ratio (Belkhatir et al., 2010), and inherent anisotropy of soil specimens (Wei and Wang, 2016) are among the main factors affecting the soil response to cyclic loading.

On the other hand, most conventional laboratory investigations focus on the macro-scale properties of soil mechanics and usually do not take into account the micro-scale variations that may occur during the loading process. While discrete element method (DEM) has proven its unique capability and is considered as a versatile tool to investigate the micro- and macro-scale behaviour of particulate assemblies (Tavarez et al., 2007, Salimi and Lashkari, 2020). In general, there are two primary methods to simulate the undrained response of fully water-saturated particulate media with DEM. The first method is known as the constant volume method, which prohibits any variations in the total volumetric strain of particulate assemblies in DEM simulations. The second approach involves combination of DEM with another numerical scheme, like the computational fluid dynamics method, to account for the presence of pore fluid in the analysis. However, this method requires significant computational requirements. Recently, Salimi and Lashkari (2020) proposed a hybrid approach called DEM- Coupled Fluid Method (CFM) to simulate the undrained response of initially anisotropic particulate assemblies under true-triaxial/triaxial conditions.

The main objective of this study is to investigate the undrained response of particulate media under recurring loading, with a focus on the inherent anisotropy of the samples. To achieve this, different soil specimens have been simulated with varying inherent anisotropy using non-spherical shapes. The DEM-CFM scheme has been employed to consider the effect of fluid-solid interaction under cyclic undrained conditions. The soil response has been evaluated for different deviatoric stress amplitudes while maintaining constant mean total stresses. Additionally, micro-scale parameters such as the coordination number, the invariant of the fabric tensor of contact orientation, and particle elongation

have been analyzed for different shear loading amplitudes.

2 BASIC ASSUMPTION OF DEM SIMULATIONS

The present study comprises simulations of particulate assemblies under undrained cyclic loading while the total mean stress p^{tot} was held constant considering a wide range of deviatoric stress amplitudes q^{amp}. The numerical calculations are conducted with the 3D Particle Flow Code (PFC3D) software (Itasca, 2014). The Coupled Fluid Method (CFM) approach was utilized to account for the undrained condition. Details about the CFM approach can be found in Salimi and Lashkari, 2020.

The linear contact model was employed to govern the particle-to-particle contact mechanism within a cubic sample (5×5×5 mm^3) enclosed by rigid boundaries. To create assemblies with distinct inherent anisotropy, 9100 elongated particles with an aspect ratio of 1.7 were generated by constructing three pebble clumps, see Figure 1 left. The chosen particle size distribution (PSD) resembles the PSD of Red Hill-110 sand. The model parameters utilized in DEM simulations are listed in Table 1.

Table 1: List of DEM parameters

Particle density	2650 [kg/m^3]
Damping ratio	0.7
Walls friction	0
Wall stiffness	10^7 [kPa]
Tangential stiffness	10^5×r§ [kPa]
Normal stiffness	10^5×r§ [kPa]
Total number of spheres	27300
Maximum diameter of particles	0.4 [mm]
Minimum diameter of particles	0.1 [mm]
Interparticle friction during shear	0.5

§ r is the pebble's radii

Initially, the particles were created with the purpose to produce transversely isotropic assemblies. The assumption for the transversely isotropic condition is that the Z direction (vertical direction) in the cartesian coordinate system is the symmetry axis and axes X and Y become a plane of symmetry. Thus, for creating an assembly with isotropic initial fabric (hereafter ISO), the particles' elongation was assigned based on the random distribution in all three axes. However, in order to generate transversely isotropic specimens (TR0, TR45, and TR90 presented in Fig. 1), the particle elongation was predefined in the Z direction and randomly distributed in the X and Y directions. In the sample denoted by TR0, the particles possess a zero inclination with respect to the horizontal plane (say ε_X-ε_Y), TR45 particles have a 45^o inclination, and TR90 particles are perpendicular to the horizontal plane. Afterwards, all samples were isotropically consolidated under 10 kPa (sample preparation stage) with different inter particle friction. Later, the interparticle friction was set to 0.5 and assemblies consolidated until 100 kPa. The interparticle friction at the sample preparation stage is assumed by trial and error in order to achieve the same void ratio of 0.640 for all samples prior to the shear stage. Figure 1 depicts the consolidated specimens, which have been color-coded to visually represent the predetermined bedding plane in a schematic manner. To maintain a quasi-static condition during the loading-unloading stage, the strain rate was maintained constant at 0.005 [1/sec] (Lopera Perez et al., 2016).

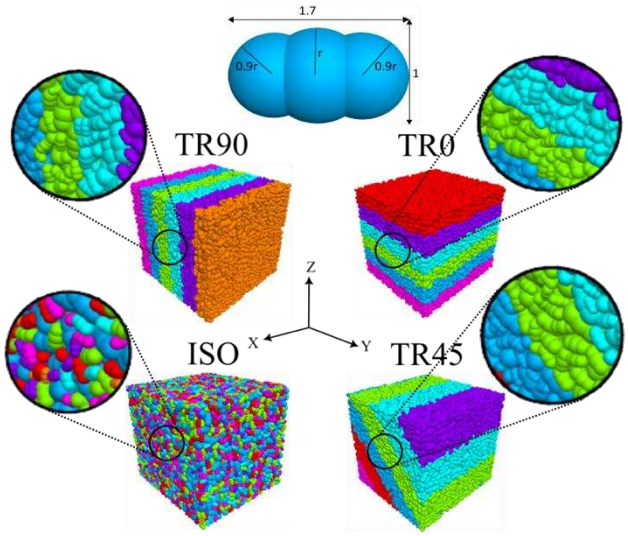

Figure 1: Schematic of particle shape and sample bedding plane.

3 MICROSCALE QUANTITIES

In DEM simulations, particles are modelled as discrete elements that interact with each other via contact forces. The coordination number (CN) of a particle is an important parameter that can affect the behavior and properties of the system. For example, a higher CN may lead to a denser and more structurally stable packing of particles, while a lower CN may result in a more fluid-like behavior (Salimi et al., 2023b). The coordination number can vary depending on the particle size, shape, and packing arrangement, as well as the simulation parameters such as the contact detection algorithm and the contact model used. Hence, the CN , which is the average contacts per particle, can be used to indicate the contribution of particles in the load-bearing microstructure of assemblies:

$$CN = \frac{1}{N_P}\sum_{N_P} n^c \quad (1)$$

where n^c and N_P denote the total number of contacts for each particle and the overall number of particles, respectively.

Another important micro-mechanical quantity can be derived based on the second invariant of the fabric tensor (**F**). Thereby, the scalar quantity for the anisotropy of granular assemblies can be calculated following:

$$\Delta^{\sqcup} = \sqrt{3\ \mathrm{dev}\ \mathbf{F}^{\sqcup} : \mathrm{dev}\ \mathbf{F}^{\sqcup}} \qquad (2)$$

where $\sqcup = c$ stands for contact orientation and $\sqcup = p$ for particle orientation of fabric tensor.

4 MACROSCALE BEHAVIOR

The ISO, TR0, TR45 and TR90 assemblies were subjected to cyclic shear under constant total stress condition. The (one-way) amplitude of the deviatoric stress q^{amp} has been varied between 45, 50, 55, 60, 65, and 70 kPa and applied only in triaxial compression ($q \geq 0$). The initial void ratio of all samples amounted 0.64 at an initially isotropic initial state of $p' = 100$ kPa. The tests ceased after shear strains of $\varepsilon_q = 13$ % as admissible deformation. Typical results of effective stress paths (q vs. p') for ISO samples are presented in Figure 2. The results show that with the increase of q^{amp}, the number of cycles to reach cyclic mobility (repeated stress loops as attractors) decreases significantly. A stress liquefaction ($p' = 0$) is not reached in such tests with $q_{min}^{compression} \geq 0$.

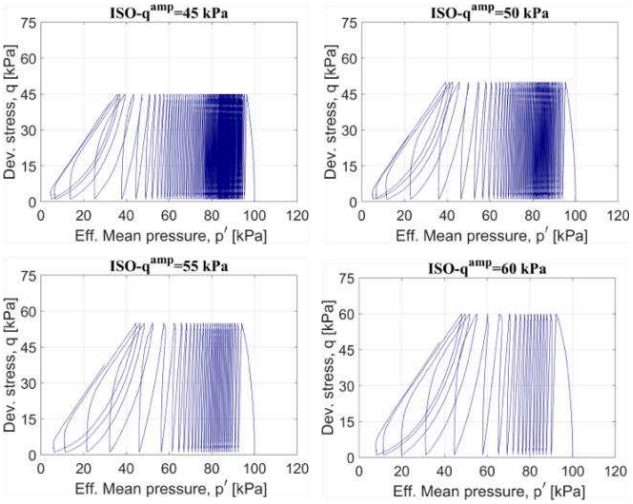

Figure 2: q vs. p' for ISO sample subjected to q^{amp}=45, 50, 55, and 60 kPa.

After a certain number of cycles, the accumulated pore water pressure reaches a stable value and thus the effective stress path repeatedly passes through a certain lens-shaped loop (attractor), which is located near the failure line (FL, known from undrained monotonic tests). For a more detailed discussion of the position of the final stress loops with respect to the FL and the phase transformation line the interested reader is referred to Salimi et al. (2023a).

On the other hand, the minimum mean effective stress reached at the attractor increases slightly with increasing deviatoric amplitude. However, the strain accumulation continues even when the stress relaxation has stopped. Figure 3 shows that the amplitude of axial strain remains almost constant throughout the cyclic mobility regardless of q^{amp}. These findings are supported by laboratory results presented for example by Wichtmann and Triantafyllidis (2014, 2016).

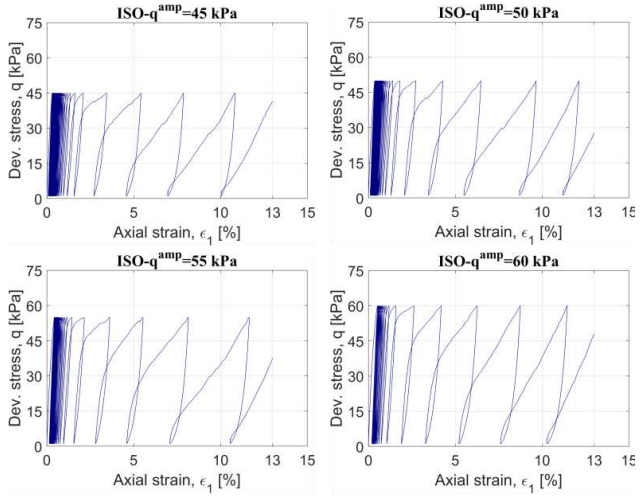

Figure 3: q vs. ϵ_1 for ISO sample subjected to q^{amp}=45, 50, 55, and 60 kPa.

Figure. 4 shows the effective stress paths of the considered anisotropic samples under q^{amp}=50 kPa. While the inclination of the stress path is rendered as more contractant for decreasing sedimentation angle, the number of cycles to reach the lens-shaped loop decreases with it. Moreover, an increase in the inclination of the bedding plane results in a larger area enclosed by the lens-shaped loop.

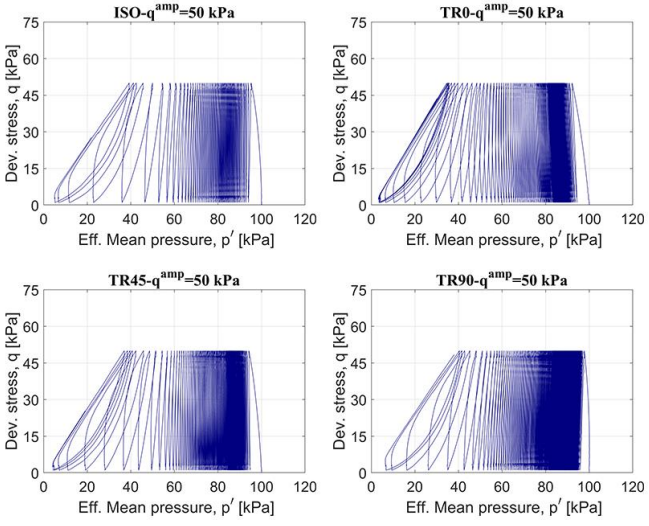

Figure 4: q vs. p' for ISO, TR0, TR45, and TR90 samples with the same void ratio (e=0.640) subjected to q^{amp}= 50 kPa.

Figure 5 illustrates the variation of q versus axial shear strain in relation to the influence of inherent anisotropy. The findings indicate that, although the axial strain amplitude remains nearly constant during cyclic mobility, it decreases with an increase in the inclination of the bedding plane.

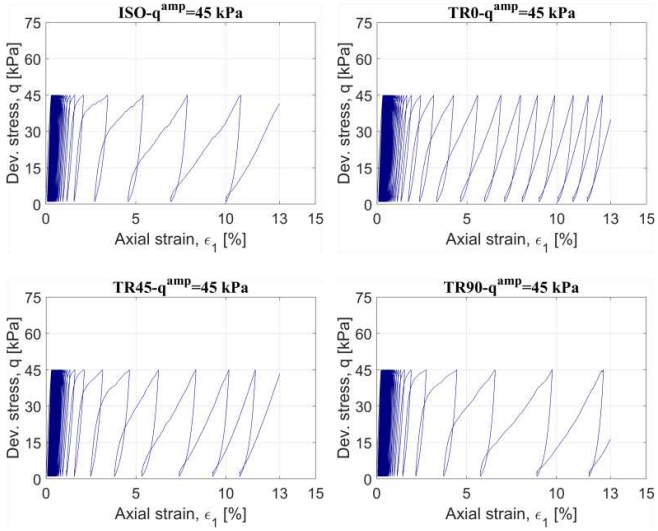

Figure 5: q vs. ϵ_1 for ISO, TR0, TR45, and TR90 samples with the same void ratio (e=0.640) subjected to q^{amp} = 45 kPa.

The development of liquefaction ratio (r_u) as ratio of excess pore water pressure to initial confining pressure ($r_u = U_w/p_0'$) with number of cycles (N) are presented in Figure 6 for the isotropic samples subjected to various q^{amp}. The results highlight, that simultaneous increase in q^{amp} is accompanied with increase in the rate of accumulation of excess pore water pressure. However, the samples which undergo lower q^{amp} reach higher amount of r_u at the end of tests, noted in the discussion of Figure 2 as well. Figure 7 illustrates r_u with number of cycles for samples with different initial anisotropy. While the rate of pore water pressure generation decreases with increasing bedding plane inclination, it can be concluded that the initial anisotropy doesn't affect the final value of r_u for a given q^{amp}.

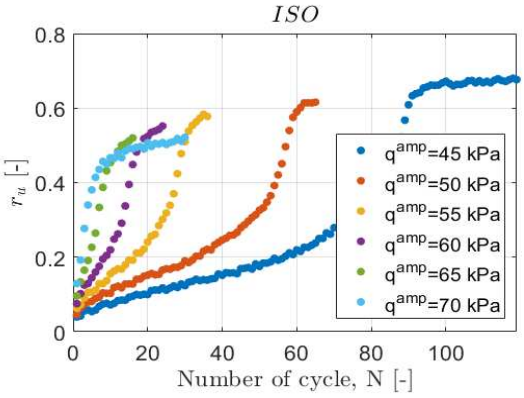

Figure. 6: r_u vs. N for ISO samples subjected to q^{amp}=45, 50, 55,60, 65, and 70 kPa.

5 MICROSCALE BEHAVIOR

The graphs presented in Figure 8 illustrate how the coordination number changes with the number of cycles for ISO, TR0, TR45, and TR90. At the initial state, all assemblies have a similar CN value of approximately 5.48, except TR90. The variation in the initial CN value for TR90 demonstrates that the arrangement of particles has an impact on CN, meaning that the same void ratio does not always lead to the same CN.

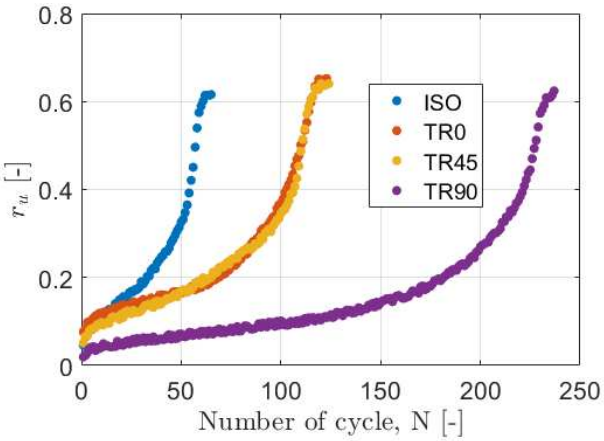

Figure 7: Variation of r_u vs. N for ISO, TR0, TR45, and TR90 samples with the same void ratio (e=0.640) subjected to q^{amp} = 50 kPa.

Moreover, it is noticeable that the CN value increases gradually with increasing N and reaches 3.5 for all assemblies by the conclusion of the test. The ISO sample has the lowest resistance (the lowest N) and the TR90 the highest one. The value of N at the end of tests for TR0, TR45, and TR90 in comparison with ISO indicates that the initial anisotropy increases the undrained resistance of granular media under repeated loading.

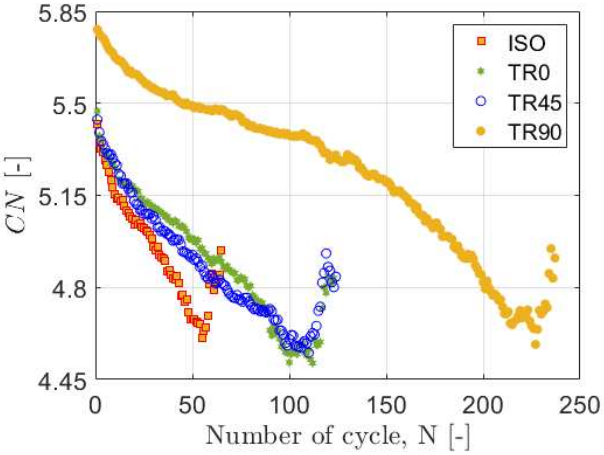

Figure 8: Evaluation of CN for ISO, TR0, TR45, and TR90 subjected to q^{amp}=45 kPa.

Figures 9 and 10 show the variation of the invariant of fabric tensor of contact orientation (Δ^c) and particle elongnation (Δ^p) vs. p' , respectively. In Figure 9, Δ^c for the ISO sample begins at 0.045 and increases gradually

until it reaches 0.24 at the end of the test. The amplitude of Δ^c grows as p' decreases, while it reaches an attractor and repeated loops at the end of the test. An examination of variations in Δ^c vs. p' for initially anisotropic assemblies reveals that the amplitude of changes in Δ^c decreases with increasing angle of bedding plane orientation. As Δ^c increases with decreasing mean stress, it can be concluded that the anisotropy of contacts increases for all assemblies, regardless of their initial inherent anisotropy.

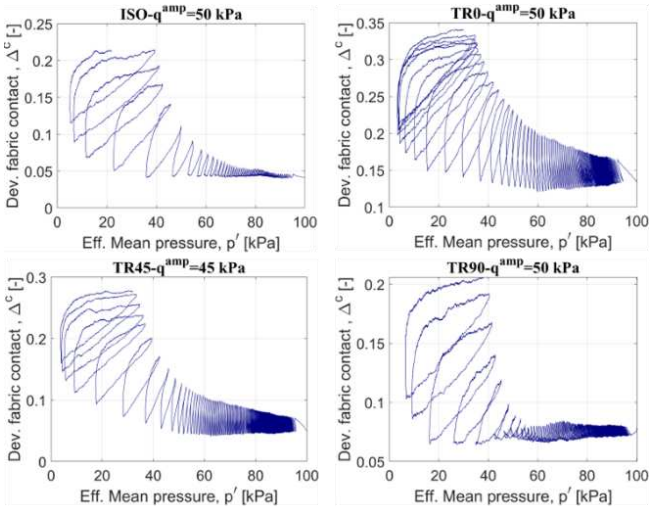

Figure 9: Δ^c vs. p' for ISO, TR0, TR45, and TR90 samples with the same void ratio (e=0.640) subjected to q^{amp}= 45 kPa.

Figure 10 presents the evaluation of invariant of fabric tensor of particle elongation versus effective mean pressure (Δ^p vs. p'). It can be observed that Δ^p initially decreases with the relaxation of mean effective stress. However, after reaching a threshold value of around $p' = 50$ kPa, any further reductions in p' result in sudden changes of Δ^p. It can be deduced that samples with a high value of Δ^p show a decreasing trend of it (TR0 and TR90), whereas samples with comparably low Δ^p tend to enhance the particle elongation anisotropy ISO and TR45). Of note, the value of q^{amp} has no significant effect on Δ^p and Δ^c.

Figure 11 compares components of fabric tensor of particle orientation for TR0 and TR45 samples under cyclic loading. The orientation of TR0 particles remain almost constant under cyclic vertical loading, while TR45 particles gradually reorient themselves to align similarly to TR0.

6 CONCLUSIONS

In order to explore the macroscopic and microscopic behavior of cross anisotropic granular assemblies of elongated particles subjected to shear under undrained constant mean total pressure, a 3D DEM-CFM scheme was employed. Therefore, samples with a bedding plane angle of 0°, 45°, 90° as well as samples with isotropic distribution of grains have been prepared. After consolidation to a mean effective stress of $p' = 100$ kPa, the samples were subjected to undrained cyclic loading in triaxial compression with deviatoric stress amplitude of q^{amp} = 45, 50, 55, 60, 65 and 70 kPa. The results indicate, that after a certain number of cycles the accumulated pore water pressure reaches a stable value and thus the effective stress path repeatedly passes through a certain lens-shaped loop (attractor). While the rate of pore water pressure generation decreases with increasing bedding plane inclination, it can be concluded that the initial anisotropy doesn't affect the final value of r_u. Nevertheless, the number of cycles to reach a specific axial strain accumulation increases with the bedding plane inclination, resulting in an increased cyclic undrained resistance of anisotropic granular media. While the coordination number indicates to reflect the evolution of excess pore water pressure, the course of the particle elongation invariant of fabric tensor seems to reflect the evolution of axial strain.

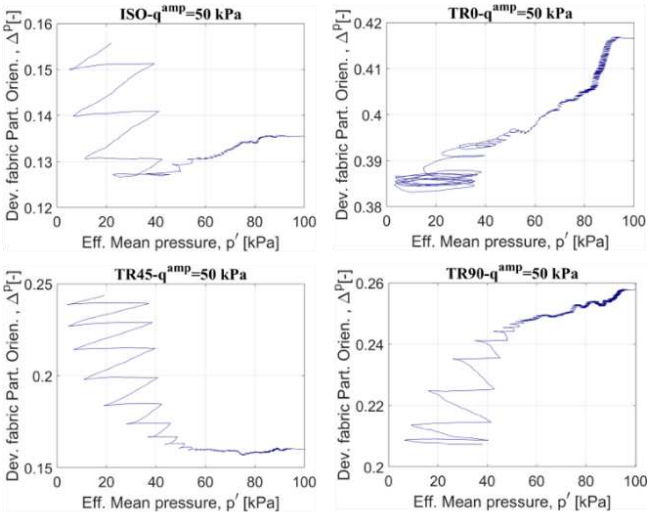

Figure 10: Δ^c vs. p' for ISO, TR0, TR45, and TR90 samples with the same void ratio (e=0.640) subjected to q^{amp}= 50 kPa.

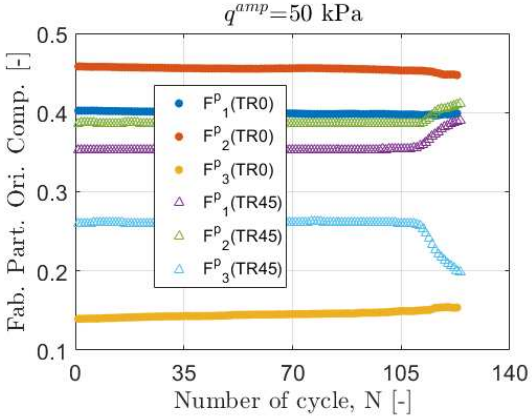

Figure 11: Evaluation of particle orientation components of fabric tensor for TR0 and TR45 samples subjected to q^{amp}= 50 kPa.

7 ACKNOWLEDGEMENTS

The presented study has been funded by the German Research Council (DFG, project No. TR 218/29-1). The authors are grateful to DFG for the financial support.

8 REFERENCES

Araei, A. A., Razeghi, H. R., Ghalandarzadeh, A., Tabatabaei, S. H. (2012). Effects of loading rate and initial stress state on stress–strain behavior of rock fill materials under monotonic and cyclic loading conditions. *Scientia Iranica*, *19*(5), 1220-1235.

Azami, A., Pietruszczak, S., Guo, P. (2010). Bearing capacity of shallow foundations in transversely isotropic granular media. *International Journal for Numerical and Analytical Methods in Geomechanics*, *34*(8), 771-793.

Belkhatir, M., Arab, A., Della, N., Missoum, H., Schanz, T. (2010). Influence of inter-granular void ratio on monotonic and cyclic undrained shear response of sandy soils. *Comptes Rendus Mecanique*, *338*(5), 290-303.

Calvetti, F., Di Prisco, C. (2010). Discrete numerical investigation of the ratcheting phenomenon in granular materials. *Comptes Rendus Mecanique*, *338*(10-11), 604-614.

Chiaro, G., Koseki, J., Sato, T. (2012). Effects of initial static shear on liquefaction and large deformation properties of loose saturated Toyoura sand in undrained cyclic torsional shear tests. *Soils and Foundations*, *52*(3), 498-510.

Elgamal, A., Yan, L., Yang, Z., Conte, J. P. (2008). Three-dimensional seismic response of Humboldt Bay bridge-foundation-ground system. *Journal of structural engineering*, *134*(7), 1165-1176.

Fiegel, G. L., Kutter, B. L. (1994). Liquefaction-induced lateral spreading of mildly sloping ground. *Journal of geotechnical engineering*, *120*(12), 2236-2243.

Itasca Consulting Group Inc. Particle flow Code in Three-Dimensions user‘s manual, Version. 5.0. Minneapolis: Itasca; 2014.

Knittel, L., Tafili, M., Tavera, C. G., Triantafyllidis, T. (2022). Influence of recent and long-lasting loading history on the cyclic behaviour of sand: confrontation of novel experimental results and established constitutive laws. *Scientific Reports*, under review.

Krathe, V. L., Kaynia, A. M. (2017). Implementation of a non‐linear foundation model for soil‐structure interaction analysis of offshore wind turbines in FAST. *Wind Energy*, *20*(4), 695-712.

Li, J., Guan, D., Chiew, Y. M., Zhang, J., Zhao, J. (2020). Temporal evolution of soil deformations around monopile foundations subjected to cyclic lateral loading. *Ocean Engineering*, *217*, 107893.

Li, B., Zeng, X., Ming, H. (2010). Seismic response of retaining wall with anisotropic backfills. In *Earth Retention Conference 3* (pp. 688-695).

Li, X. S., Dafalias, Y. F. (2002). Constitutive modeling of inherently anisotropic sand behavior. *Journal of Geotechnical and Geoenvironmental Engineering*, *128*(10), 868-880.

Lu, X., Huang, M., Qian, J. (2011). The onset of strain localization in cross-anisotropic soils under true triaxial condition. *Soils and foundations*, *51*(4), 693-700.

Lopera Perez, J. C., Kwok, C. Y., O‘Sullivan, C., Huang, X., Hanley, K. J. (2016). Exploring the micro-mechanics of triaxial instability in granular materials. *Géotechnique*, 66(9): 725-740.

Machaček, J., Staubach, P., Tafili, M., Zachert, H., Wichtmann, T. (2021). Investigation of three sophisticated constitutive soil models: From numerical formulations to element tests and the analysis of vibratory pile driving tests. *Computers and Geotechnics*, 138: 104276.

Qin, J., Zeng, X., Ming, H. (2016). Centrifuge modeling and the influence of fabric anisotropy on seismic response of foundations. *Journal of geotechnical and geoenvironmental engineering*, *142*(3), 04015082.

Salimi, M. J., Lashkari, A. (2020). Undrained true triaxial response of initially anisotropic particulate assemblies using CFM-DEM. *Computers and Geotechnics*, *124*, 103509.

Salimi, M., Tafili, M., Prada-Sarmiento, L.F., Triantafyllidis, T., Wichtmann, T. (2023). Undrained Cyclic True Triaxial Tests Considering the inherent Anisotropy: DEM-CFM approach. Submitted for *Geotechnique*.

Salimi, M., Lashkari, A., Tafili, M. (2023). DEM investigation on flow instability of particulate assemblies under coupling between volumetric and axial strains. *Acta Geotechnica* (under review).

Tafili, M., Wichtmann, T. (2022). Finite Element Modelling of Tunnel Settlements Under Cyclic Loading. In Challenges and Innovations in Geomechanics: Proceedings of the 16th International Conference of IACMAG, 3: 150-157. Cham: Springer International Publishing.

Tavarez, F. A., Plesha, M. E. (2007). Discrete element method for modelling solid and particulate materials. *International journal for numerical methods in engineering*, *70*(4), 379-404.

Tokimatsu, K., Suzuki, H. (2004). Pore water pressure response around pile and its effects on py behavior during soil liquefaction. *Soils and Foundations*, *44*(6), 101-110.

Tohumcu Özener, P., Özaydın, K., Berilgen, M. M. (2009). Investigation of liquefaction and pore water pressure development in layered sands. *Bulletin of Earthquake Engineering*, *7*, 199-219.

Van den Eijnden, A. P., Bésuelle, P., Collin, F., Chambon, R., Desrues, J. (2017). Modeling the strain localization around an underground gallery with a hydro-mechanical double scale model; effect of anisotropy. *Computers and Geotechnics*, *85*, 384-400.

Wei, J., Wang, G. (2016). Evolution of fabric anisotropy in cyclic liquefaction of sands. *Journal of Micromechanics and Molecular Physics*, *1*(03n04), 1640005.

Wichtmann, T., Triantafyllidis, T. (2014). Stress attractors predicted by a high-cycle accumulation model confirmed by undrained cyclic triaxial tests. *Soil Dynamics and Earthquake Engineering*, 69(2): 125–137.

Wichtmann, T., Triantafyllidis, T. (2016). An experimental database for the development, calibration and verification of constitutive models for sand with focus to cyclic loading: part I—tests with monotonic loading and stress cycles. *Acta Geotechnica*, 11: 739-761.